INTERNATIONAL JOURNAL FOR NUMERICAL METHODS IN FLUIDS
Int. J. Numer. Meth. Fluids 2005; **47**:1053–1059
Published online 24 January 2005 in Wiley InterScience (www.interscience.wiley.com). DOI: 10.1002/fld.852

Anisotropic, isothermal, turbulent swirling flow in a complex combustor geometry

L. N. Jones[1], P. H. Gaskell[1], H. M. Thompson[1], X. J. Gu[2,*,†] and D. R. Emerson[2]

[1]*Engineering Fluid Mechanics Research Group, School of Mechanical Engineering, University of Leeds, U.K.*
[2]*Computational Engineering Group, CLRC Laboratories, Daresbury, Warrington, U.K.*

SUMMARY

The performance of popular second moment closure (LRR, SSG) turbulence models is assessed and compared against experimental data for anisotropic swirling flow in a cylindrical combustion chamber. In contrast to previous studies, where the dissipation anisotropy is correlated with the stress anisotropy, the benefit of approximating the former for swirling flows in terms of the mean strain and vorticity is investigated. Second moment closure models are found to predict mean and turbulent flow quantities reasonably well everywhere except near the wall. The anisotropic dissipation model is found to improve prediction of mean flow quantities near the chamber axis and acts to preserve turbulence further downstream. Copyright © 2005 John Wiley & Sons, Ltd.

KEY WORDS: dissipation anisotropy; second moment closure; swirl

1. INTRODUCTION

Swirl is a very important flow feature with many industrial applications, a key distinction being its role in promoting mixing and flame stability in combustion chambers. Previous numerical studies of turbulent, swirling flows have highlighted their anisotropic nature and shown that although the performance of two-equation turbulence models can be improved by the inclusion of non-linear terms, more accurate simulations require determination of the Reynolds stresses [1–3]. To account for flow history, solution of the full Reynolds stress (RS) transport equation is required [4].

Much of the previous research directed at improving the performance of second moment, or RS, Closure models have focussed on the pressure–strain correlation (PSC), the most popular form being that of Launder *et al.* [5], commonly referred to as the LRR model, which

*Correspondence to: X. J. Gu, Computational Engineering Group, CLRC Laboratories, Daresbury, Warrington, U.K.
†E-mail: x.j.gu@dl.ac.uk

Contract/grant sponsor: EPSRC
Contract/grant sponsor: School of Mechanical Engineering

Received 27 April 2004
Revised 28 September 2004
Accepted 12 November 2004

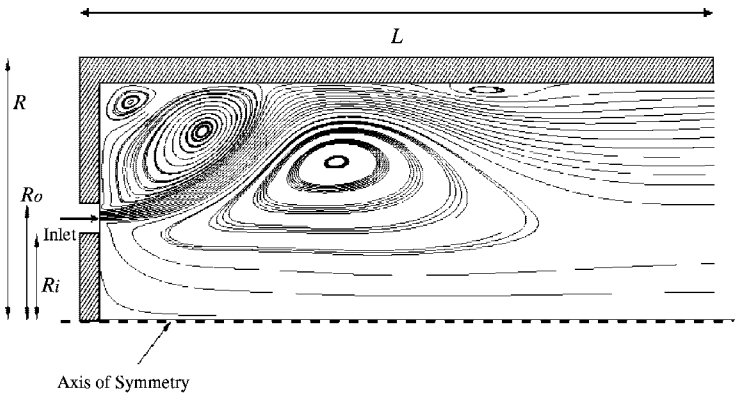

Figure 1. Flow schematic with computed flow field; LRR model.

represents the PSC as a non-linear combination of the Reynolds stresses and mean strains with a *linear* anisotropic term. Speziale *et al.* [6] subsequently introduced a PSC, quadratic in the anisotropy tensor, with the claim that their so-named SSG model is more effective in capturing the non-linear dynamics of turbulence. Other, more complex models such as the two component limit model of Craft and Launder [7] appear to be as yet untested in swirling flows.

Although the above RS models account for RS anisotropies, the dissipation rate tensor is normally modelled in an isotropic manner. This is despite recent evidence that dissipation anisotropy may be more than 50% greater than the stress anisotropy even in simple homogeneous shear flow [8]. Although few studies have applied anisotropic dissipation rate models (ADRMs) in swirling flow ([9] with a high Reynolds number formulation and [10] with a low Reynolds number model), non-rotating flows have been successfully predicted using models that correlate the dissipation anisotropy with the stress anisotropy [11], while the model of Speziale and Gatski [12], based on the mean strain and vorticity, has performed well for rotating flow.

The present study assesses the performance of the LRR and SSG models, and the latter also inclusive of Speziale and Gatski's [12] ADRM, for predicting isothermal flow in a cylindrical combustion chamber, see Figure 1, of radius, $R = 0.024$ m, and length $L = 1.5$ m [13]. Air is injected through an inlet whose inner and outer radii from the axis are $R_\mathrm{i} = 10$ mm and $R_\mathrm{o} = 11$mm, respectively, and the inlet swirl velocity W is given by a piecewise linear function, approximating a triangular profile with values at the inner and outer radii equal to zero. Flow with axial mean inlet velocity of $U_{av} = 30\,\mathrm{m\,s^{-1}}$ was considered, with a swirl number defined by $S = \int_{R_\mathrm{i}}^{R_\mathrm{o}} WUr^2\,\mathrm{d}r / R_\mathrm{i} \int_{R_\mathrm{i}}^{R_\mathrm{o}} U^2 r\,\mathrm{d}r = 0.53$.

2. MATHEMATICAL MODEL AND METHOD OF SOLUTION

Flow is investigated by solving the RANS equations, from which the transport equation (1) for the RSes, $\tau_{ij} = \overline{u_i u_j}$, are obtained; U_i are the mean flow velocities, Π_{ij} the PSC, ε_{ij} the dissipation rate tensor and C_{ijk} the turbulent diffusion terms. Here, Π_{ij} is modelled using the LRR (3) or SSG (4) models and C_{ijk} via the gradient diffusion hypothesis. The LRR model

uses additional wall reflection terms from Gibson and Launder [14] while the SSG model is used without such terms, relying instead on its non-linear form to account for wall effects.

Here, the anisotropic dissipation rate model of Speziale and Gatski [12] is used with the dissipation rate tensor given by Equation (5) in terms of the turbulent kinetic energy dissipation rate, ε, governed by Equation (2). The dissipation anisotropy tensor, d_{ij}, used here is given by Equation (6) and is the computationally efficient, algebraic form derived by Speziale and Gatski [12] in terms of the mean strain and vorticity tensors. The transport equation for the dissipation rate is sensitised to the anisotropy of dissipation through the production of dissipation term and the coefficient $C^*_{\varepsilon 1}$ in Equation (9) where $\alpha = \frac{3}{4}(\frac{14}{11}\alpha_3 - \frac{16}{33})$. The closure coefficients for the model are: $C_\varepsilon = 0.15$, $C_{\varepsilon 1} = 1.0$, $C_{\varepsilon 2} = 1.83$, $C_{\varepsilon 5} = 5.80$, $\alpha_3 = 0.6$ and $C^*_\mu = 0.094$. For other closure coefficients, see References [5, 6]. Logarithmic wall functions are employed, an assumption that is supported by the experimental results of Kitoh [15] for swirling flow in a long cylinder. The RSes at the near-wall nodes are calculated based on values of turbulent kinetic energy, k, as shown in Reference [16]. The values of k and the integral length scale at the inlet boundary were given by Al-Masseeh and the value of the dissipation rate was estimated from them accordingly [2].

With the tensors of the RS anisotropy a_{ij}, the mean rate of strain $\bar{S}_{ij}$ and the mean vorticity $\bar{W}_{ij}$, the models employed in the present study are expressed as:

$$U_k \frac{\partial \tau_{ij}}{\partial x_k} = P_{ij} + \Pi_{ij} - \varepsilon_{ij} - \frac{\partial}{\partial x_k} C_{ijk} + \nu \nabla^2 \tau_{ij} \tag{1}$$

$$U_i \frac{\partial \varepsilon}{\partial x_{\mathrm{i}}} = C_\varepsilon \frac{\partial}{\partial x_k}\left(\frac{k}{\varepsilon}\overline{u_k u_l}\frac{\partial \varepsilon}{\partial x_l}\right) - C^*_{\varepsilon 1}\frac{\varepsilon}{k}\overline{u_i u_k}\frac{\partial U_i}{\partial x_k} - C_{\varepsilon 2}\frac{\varepsilon^2}{k} \tag{2}$$

$$\Pi_{ij,\mathrm{LRR}} = -C_1 \varepsilon a_{ij} - \frac{C_2 + 8}{11}\left(P_{ij} - \frac{2}{3}P\delta_{ij}\right) - 2\frac{30C_2 - 2}{55}k\bar{S}_{ij} - \frac{8C_2 - 2}{11}\left(D_{ij} - \frac{2}{3}P\delta_{ij}\right) \tag{3}$$

$$\Pi_{ij,\mathrm{SSG}} = -\left(C_1 + C^*_1\frac{P}{\varepsilon}\right)\varepsilon a_{ij} + C_2\varepsilon\left(a_{ik}a_{kj} - \frac{1}{3}a_{mn}a_{mn}\delta_{ij}\right) + \left(C_3 - C^*_3 II^{\frac{1}{2}}\right)k\bar{S}_{ij} + C_4 k\left(a_{ik}\bar{S}_{jk} + a_{jk}\bar{S}_{ik} - \frac{2}{3}a_{mn}\bar{S}_{mn}\delta_{ij}\right) + C_5 k(a_{ik}\bar{W}_{jk} + a_{jk}\bar{W}_{ik}) \tag{4}$$

$$P_{ij} = -\tau_{ik}\frac{\partial U_j}{\partial x_k} - \tau_{jk}\frac{\partial U_i}{\partial x_k}, \quad P = \frac{1}{2}P_{kk}, \quad D_{ij} = -\tau_{ik}\frac{\partial U_k}{\partial x_j} - \tau_{jk}\frac{\partial U_k}{\partial x_i}$$

$$\varepsilon_{ij} = \tfrac{2}{3}\varepsilon\delta_{ij} + 2\varepsilon d_{ij} \tag{5}$$

$$d_{ij} = -2C_{\mu\varepsilon}\left[\frac{k}{\varepsilon}\bar{S}_{ij} + \frac{1}{\beta}\left(\frac{7}{11}\alpha_3 + \frac{1}{11}\right)\frac{k^2}{\varepsilon^2}\left(\bar{S}_{ik}\bar{W}_{kj} + \bar{S}_{jk}\bar{W}_{ki}\right) + \frac{1}{\beta}\left(\frac{30}{11}\alpha_3 - \frac{2}{11}\right)\frac{k^2}{\varepsilon^2}\left(\bar{S}_{ik}\bar{S}_{kj} - \frac{1}{3}\bar{S}_{kl}\bar{S}_{kl}\delta_{ij}\right)\right] \tag{6}$$

$$C_{\mu\varepsilon} = \frac{1}{15\beta}\left[1 + 2\left(\frac{\frac{7}{11}\alpha_3 + \frac{1}{11}}{\beta}\right)^2 \xi^2 - \frac{2}{3}\left(\frac{\frac{15}{11}\alpha_3 - \frac{1}{11}}{\beta}\right)^2 \eta^2\right]^{-1} \tag{7}$$

$$\eta = (\bar{S}_{ij}\bar{S}_{ij})^{1/2}\frac{k}{\varepsilon}, \qquad \xi = (\bar{W}_{ij}\bar{W}_{ij})^{1/2}\frac{k}{\varepsilon}, \qquad \beta = C_{\varepsilon 5} + 2C_{\mu}^{*}\eta^2 - 1 \tag{8}$$

$$C_{\varepsilon 1}^{*} = C_{\varepsilon 1} + \frac{2(1+\alpha)}{15C_{\mu}^{*}}\left[\frac{\beta}{\beta^2 - \frac{2}{3}(\frac{8}{11})^2\eta^2 + 2(\frac{26}{55})^2\xi^2}\right] \tag{9}$$

Two high-order discretization schemes, namely SMART [17] and CUBISTA [18] were employed to approximate convective transport, both of which incorporate the convective boundedness criterion (CBC) of Gaskell and Lau [17] to achieve physically bounded interpolations. The computational mesh employed is block-structured and all results were obtained using 100 axial and 56 radial nodes to ensure mesh independence. Solutions were found using the well known SIMPLE procedure and collocated storage of variables.

3. RESULTS

A streamline plot of the computed flow field is shown in Figure 1, illustrating the primary recirculation zone along the cylindrical chamber, with two corner recirculations above the inlet. Computed mean flow quantities are shown in Figure 2 at the $x = 5$ and 200 mm axial locations and compared with the experimentally obtained values of Al-Masseeh [13].

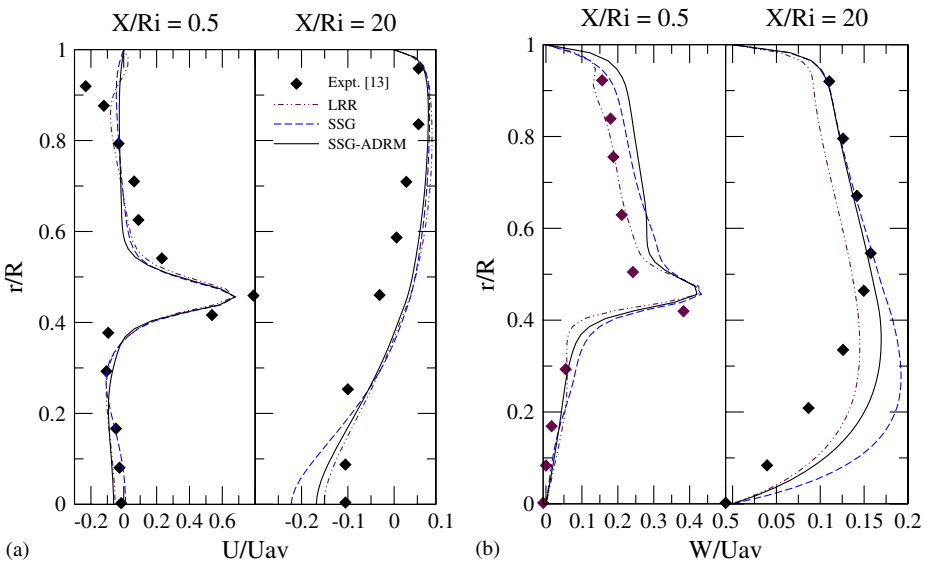

Figure 2. Predicted and measured radial flow profiles for: (a) mean axial velocity; and (b) mean tangential velocity.

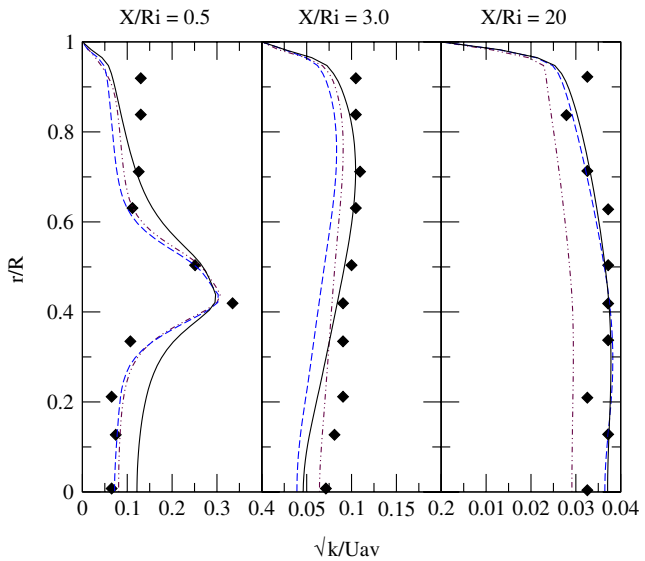

Figure 3. Predicted and measured radial flow profiles for k (key as in Figure 2).

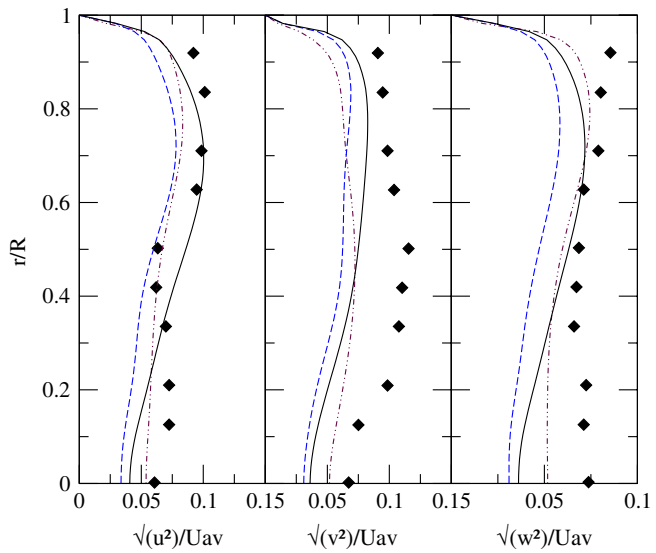

Figure 4. Predicted and measured normal stresses at $x/R_i = 3$ (key as in Figure 2).

In Figure 2(a), both RS models are seen to perform well near the chamber axis and inlet jet but less so near the wall. Here the LRR model predicts an erroneous positive axial velocity, signifying the incorrect position of the corner recirculation shown in Figure 1. The ADRM improves the prediction of the SSG model in the region between the chamber axis and the jet. Between the jet and the wall, however, the prediction is less satisfactory.

In Figure 2(b), the same trends are seen for the tangential velocity, W, above and below the jet region.

Figure 3 shows the corresponding results for the turbulent kinetic energy, k. Here, the LRR and SSG models perform well except in the near wall region. Surprisingly, the addition of anisotropic dissipation slightly degrades the performance of the SSG model at the chamber axis near the inlet jet. This is due to the positive strain rates in this region, leading to negative diagonal components of d_{ij} from Equation (6), thus reducing dissipation through (5) and hence overestimating k.

Figure 4 compares the predicted normal RS components against those measured by Al-Masseeh at $x/R_i = 3$. These components are generally predicted well, except for the v^2 component, which is slightly underpredicted. All three components are underpredicted close to the central axis, especially when using the SSG model. The addition of the ADRM facilitates a redistribution of dissipation from the normal to the shear stress components, via Equation (5), and acts to improve the agreement with experiment by preserving turbulence further downstream, as also seen in Figure 3.

4. DISCUSSION

For the flow investigated, the LRR and SSG models both predict mean and turbulent flow quantities reasonably well except near the wall. The ADRM of Speziale and Gatski generally improves mean flow predictions, particularly near the chamber axis. Although numerical experiments have highlighted an insensitivity to the sign of the mean strain and vorticity, this study has revealed the need for further investigation into the effects of the present ADRM on production (through coefficient $C^*_{\varepsilon 1}$ in (9)) and redistribution of dissipation. Future studies will also investigate the effect of wall boundary conditions and assess the performance of different ADRMs [19].

ACKNOWLEDGEMENTS

The authors would like to thank EPSRC for their support of the CCP12 programme and L. N. J. gratefully acknowledges the financial support of the School of Mechanical Engineering through a School PhD studentship.

REFERENCES

1. Chen JC, Lin CA. Computations of strongly swirling flows with second moment closures. *International Journal for Numerical Methods in Fluids* 1999; **30**:493–508.
2. Hogg S, Leschziner MA. Computation of highly swirling confined flow with a Reynolds-stress turbulence model. *AIAA Journal* 1989; **27**:57–67.
3. Hogg S, Leschziner MA. Second-moment closure calculations of strongly swirling confined flow with large density gradients. *International Journal of Heat and Fluid Flow* 1989; **10**:16–27.
4. Hanjalic K. Second-moment closures for CFD: needs and prospects. *International Journal of CFD* 1999; **12**: 67–97.
5. Launder BE, Reece GJ, Rodi W. Progress in the development of a Reynolds-stress turbulence closure. *Journal of Fluid Mechanics* 1975; **63**(3):537–566.
6. Speziale CG, Sarkar S, Gatski TB. Modelling the pressure–strain correlation of turbulence: an invariant dynamical systems approach. *Journal of Fluid Mechanics* 1991; **227**:245–272.
7. Craft TJ, Launder BE. Principles and performance of TCL-based second-moment closures. *Flow, Turbulence and Combustion* 2001; **66**:355–372.

8. So RMC, Zhao CY, Gatski TB. Predicting buoyant shear flows using anisotropic dissipation rate models. *Flow, Turbulence and Combustion* 1999; **63**:193–221.
9. Lu P, Semiao V. A new second moment closure approach for turbulent swirling confined flows. *International Journal for Numerical Methods in Fluids* 2003; **41**:133–150.
10. Jakirlic S, Hanjalic K, Tropea C. Modeling rotating and swirling turbulent flows: a perpetual challenge. *AIAA Journal* 2002; **40**:1984–1996.
11. Jovanovic J, Otic I, Bradshaw P. On the anisotropy of axisymmetric strained turbulence in the dissipation range. *Journal of Fluids Engineering* 2003; **125**:401–413.
12. Speziale CG, Gatski TB. Analysis and modelling of anisotropies in the dissipation rate of turbulence. *Journal of Fluids Mechanics* 1997; **344**:155–180.
13. Al-Masseeh WAA. Fundamental aspects of combustion in swirling flow. *Ph.D. Thesis*, University of Leeds, 1991.
14. Gibson MM, Launder BE. Ground effects on pressure fluctuations in the atmospheric boundary layer. *Journal of Fluid Mechanics* 1978; **86**:491–511.
15. Kitoh O. Experimental study of turbulent swirling flow in a straight pipe. *Journal of Fluid Mechanics* 1991; **225**:445–479.
16. Lien SF, Leschziner MA. A general nonorthogonal collocated finite-volume algorithm for turbulent-flow at all speeds incorporating 2nd-moment turbulence-transport closure. 1. Computational implementation. *Computer Methods in Applied Mechanics and Engineering* 1994; **114**:123–148.
17. Gaskell PH, Lau AKC. Curvature compensated convective transport: SMART, a new boundedness preserving transport algorithm. *International Journal for Numerical Methods in Fluids* 1988; **8**:617–641.
18. Alves MA, Oliveira PJ, Pinho FT. A convergent and universally bounded interpolation scheme for the treatment of advection. *International Journal for Numerical Methods in Fluids* 2003; **41**:47–75.
19. Jakirlic S, Hanjalic K. A new approach to modelling near-wall turbulence energy and stress dissipation. *Journal of Fluids Mechanics* 2002; **459**:139–166.

